

On a kinematically exact rod model for thin-walled open section members

Marcos P. Kassab¹, Eduardo M.B. Campello¹

¹*Dept. of Structural and Geotechnical Engineering, Polytechnic School, University of São Paulo
P.O. Box 61548, 05424-970, São Paulo, SP, Brazil
marcos.kassab@usp.br, campello@usp.br*

Abstract. In the context of frame structures, kinematically exact rod models are pivotal to correctly describe critical loads and post-critical behaviour. For thin-walled open-section members, such formulations need to take cross-sectional warping into account, since it becomes a relevant load-carrying mechanism due to the very small torsion stiffness of such members. Most thin-walled rod models available in the literature consider only the so-called primary warping, which is the warping in the direction of the cross-section's walls lengths. The walls' thickness warping, or secondary warping, is typically neglected. Although primary warping generally suffices to properly capture the rod's deformation, there are particular cases wherein secondary warping becomes relevant, and to which existing models often fail to perform. This work develops a kinematically exact rod model for thin-walled open section members taking into account both primary and secondary cross-sectional warpings. Advanced elastic constitutive equations are then incorporated in order to enable full bending, compression and torsional strain couplings in the finite strain regime. The model is implemented in an in-house finite element program and its outcomes are validated against reference solutions obtained using hierarchically higher order formulations, having as reference large deformation ANSYS's shell 181 elements.

Keywords: Kinematically exact rod models; thin-walled rods; open section members; secondary warping

1 Introduction

One-dimensional linear rod models were the first attempt in science and engineering to mathematically represent real life structures. Ranging from Bernoulli-Euler's to Timoshenko's and Vlasov's theories, and although very convenient, they are unsuited if one is interested in evaluating flexible structures and post-critical behaviour. These models can be found in many textbooks (see [1] and [2], for example).

The first (three-dimensional) kinematically exact rod model was presented by Simo [3] and Simo and Vu-Quoc [4], where a Timoshenko-like assumption for the cross-sectional shearing w.r.t. the rod axis was followed. The rotational degrees-of-freedom (DOFs) were exactly treated through the Euler-Rodrigues formula, and this was a major breakthrough at the time. Simo and Vu-Quoc [5] also advanced towards considering a warping function, especially useful for torsion-dominated problems. A wide array of nonlinear rod models has been developed in the literature since then, many of which directly derived from Simo's works. In order to mention a few interesting formulations, particularly related to the purpose of this paper, the reader might consult the works of [6]–[13].

Still, when it comes to thin-walled open-section members, existing formulations often struggle to simultaneously predict critical loads *and* post critical behaviour, to which torsion and warping become relevant to the buckling mode. Most of these models typically consider only the so-called primary warping, which is the warping in the direction of the cross-section's walls lengths, and ignore the warping in the thickness direction, or secondary warping. The lack of secondary warping, combined with the use of unsuited material laws for large deformations, may explain the difficulties of these models in the pursuit of post-critical solutions. Recently, Campello and Lago [11] incorporated a more elaborate assumption for the warping deformation, together with a more advanced constitutive law for large strains. However, the proposed warping function was only suitable to

certain bi-symmetric cross-sections (although this was not detected at the time), which were the tested cases.

In this context, this work develops a geometrically-exact rod model that correctly accounts for both primary and secondary warpings for arbitrary (symmetric and non-symmetric) thin-walled open sections. We then adopt the Saint-Venant's material law and derive an advanced constitutive equation, whereby all strain terms in the stress-strain relation are retained, arriving at a robust 7-DOF model for thin-walled open-section members. The model is implemented into PEFSYS, a nonlinear finite element program for static and dynamic analysis under development at the Department of Structural and Geotechnical Engineering of the University of São Paulo, and is validated against reference solutions obtained from the literature and also with ANSYS's shell 181 elements. This work is an intermediate step of a larger work, which aims to incorporate the truly large-strain, neo-Hookean Simo-Ciarlet's material law at the constitutive equation.

The following notation is adopted here: lowercase italic Latin or Greek letters ($a, b, \dots, \alpha, \beta, \dots$) denote scalar quantities, lowercase bold-italic Latin or Greek letters ($\mathbf{a}, \mathbf{b}, \dots, \boldsymbol{\alpha}, \boldsymbol{\beta}, \dots$) denote vectors, and capital bold-italic Latin or Greek letters ($\mathbf{A}, \mathbf{B}, \dots$) denote second-order tensors. Implicit summation convention is used throughout the text. When indices are Greek letters, they range from 1 to 2; when they are Latin letters, from 1 to 3. Scalar, cross and dyadic products are represented by “ \cdot ”, “ \times ” and “ \otimes ”, respectively. Symbol $\delta(\circ)$ denotes a virtual quantity (or, equivalently, a variation), whereas $(\circ)^r$ denotes a quantity in the reference configuration.

2 The Rod Model

Using a total Lagrangean description, based on the general (multi-parameter) kinematically exact beam model of Pimenta and Campello [12], a 7-DOF model can be developed. As basic assumptions, the cross-sections' displacements are a sum of a rigid body displacement (defined by the beam axis' displacements \mathbf{u} and Euler rotation vector $\boldsymbol{\theta}$, on the global Cartesian system, comprising 6 DOFs) and an out-of-plane warping displacement. The latter is given by the product of a warping intensity parameter (p , the 7th DOF) and a shape function (ψ), which depends solely on the cross-section's geometry. The constitutive equation may be derived from the Saint-Venant's material law, retaining some [8] or all [11] of the higher-order strain terms (opposed to the often used linear constitutive equation, as e.g. in [3]–[5] and [7]). In [11], this model is particularized to the case of 7-DOF models and “exact” constitutive equation (i.e., with all strain terms retained), with numerical cross-section integration for computation of the stress-resultants, similarly to the approach adopted in the current work. Here, this is achieved by discretizing each of the cross-section's walls on rectangular cells, and then integrating the desired function with the standard composed Simpson's method. In this section, a brief description is shown. For more details, it is suggested that the reader consults the above-mentioned references, especially [11]. The model's solution can be achieved through a standard (Lagrangean, isoparametric) beam finite element, numerically integrated along the element's axis with reduced integration to avoid shear locking. Incremental loading is implemented for the solution. Each one of the incremental load steps is solved using Newton's method.

2.1 Kinematical description

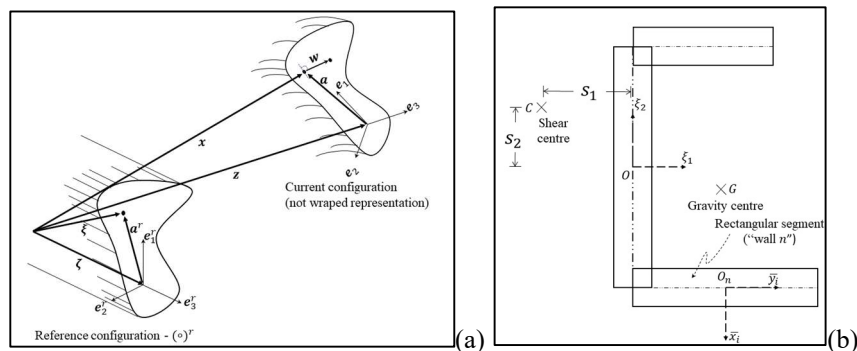


Figure 1. (a) Rod kinematics and (b) representation of a thin-walled cross-section

Assuming a straight rod initial configuration, with a local orthonormal system $\{\mathbf{e}_1^r, \mathbf{e}_2^r, \mathbf{e}_3^r\}$, with \mathbf{e}_3^r coinciding

with the reference rod's axis (see Fig. 1a), the position of every material point in the reference configuration can be described by

$$\boldsymbol{\xi} = \zeta \mathbf{e}_3^r + \mathbf{a}^r, \quad \zeta \in \Omega = [0, L]. \quad (1)$$

In the current configuration, the position of every point is represented by

$$\mathbf{x} = \mathbf{z} + \mathbf{a} + \mathbf{w}, \quad (2)$$

where $\mathbf{u} = \mathbf{z} - \boldsymbol{\zeta}$ represents the axis displacement, $\mathbf{a} = \mathbf{Q}\mathbf{a}^r$ the cross-section's displacements due to rotation and $\mathbf{w} = p\psi\mathbf{e}_3$ the warping displacement, for a given rotation tensor (\mathbf{Q}), warping function (ψ) and warping intensity (p). For each cross-sectional wall n , an orthonormal local system (\bar{x}_n, \bar{y}_n) is assigned (see Fig. 1b), as this will be useful for the definition of the warping function later on. The rotation field is parametrized using Euler-Rodrigues equation, exactly as done in [3], [7], [10], for example. It is useful to group the model's DOFs $\mathbf{u}, \boldsymbol{\theta}$ and p into a generalized displacement vector, $\mathbf{d} = [\mathbf{u}, \boldsymbol{\theta}, p]^T$. The deformation gradient \mathbf{F} is obtained from eq. (2), and reads

$$\mathbf{F} = \frac{\partial \mathbf{x}}{\partial \boldsymbol{\xi}} = \mathbf{Q}(\mathbf{I} + \psi_{,\alpha} p \mathbf{e}_3^r \otimes \mathbf{e}_\alpha^r + \boldsymbol{\gamma}_3^r \otimes \mathbf{e}_3^r) = \mathbf{Q}\mathbf{F}^r, \quad \text{with} \quad (3)$$

$$\boldsymbol{\gamma}_3^r = \boldsymbol{\eta}^r + \boldsymbol{\kappa}^r \times (\mathbf{a}^r + \psi p \mathbf{e}_3^r) + \psi p' \mathbf{e}_3^r \quad \text{and} \quad \boldsymbol{\eta}^r = \mathbf{Q}^T \mathbf{z}' - \mathbf{e}_3^r \quad \text{and} \quad \boldsymbol{\kappa}^r = \boldsymbol{\Gamma}^T \boldsymbol{\theta}'. \quad (4)$$

Tensor $\boldsymbol{\Gamma}$, required in eq. (4), is a sub-product of the derivative of the rotation tensor, and its definition can be found in [3], with a different notation, or in [7]. The above strain quantities can be assigned to a generalized strain vector, $\boldsymbol{\varepsilon}^r = [\boldsymbol{\eta}^r, \boldsymbol{\kappa}^r, p, p']^T$.

2.2 Equilibrium: weak form

The virtual work theorem is invoked, imposing the rod's equilibrium:

$$\delta W = \delta W_{int} - \delta W_{ext} = 0 \text{ in } \Omega, \forall \delta \mathbf{d} | \delta \mathbf{d}(0) = \delta \mathbf{d}(L) = \mathbf{o}. \quad (5)$$

The Fréchet derivative of eq. (5) with respect to \mathbf{d} results in the tangent operator of the equilibrium, and will be directly used on the finite element method's formulation, as already reported in [3], [7], [8] and other references that use a similar description for their models. The internal virtual work can be calculated, using the first Piola-Kirchhoff stress tensor and the deformation gradient conjugate pair $\{\mathbf{P}, \mathbf{F}\}$, as

$$\delta W_{int} = \int_{\Omega} \int_A (\mathbf{P} : \delta \mathbf{F}) dA d\zeta = \int_{\Omega} (\boldsymbol{\sigma}^r \cdot \delta \boldsymbol{\varepsilon}^r) d\zeta, \quad (6)$$

wherein $\boldsymbol{\sigma}^r = [\mathbf{n}^r, \mathbf{m}^r, Q, B]^T$ is the generalized stress resultants vector and $\delta \boldsymbol{\varepsilon}^r$ has an analogous definition as $\boldsymbol{\varepsilon}^r$. The interpretation of those quantities is the usual: vector \mathbf{n} contains the shear (V_α) and axial (N) forces, whereas \mathbf{m} contains the bending (M_α) and torsional (T) moments. The warping-related quantities are the bi-shear (Q) and bi-moment (B). These resultants are obtained through cross-sectional integration of the column-vectors of the back-rotated stresses $\mathbf{P}^r = \mathbf{Q}^T \mathbf{P}$ (see [11]). It is necessary to obtain the variation of eq. (3) with respect to \mathbf{d} . This step can be seen in [7], [8] and will not be reproduced here. As demonstrated in [3], $\delta \boldsymbol{\varepsilon}^r$ can be written in the form $\delta \boldsymbol{\varepsilon}^r = \boldsymbol{\Psi} \boldsymbol{\Delta} \delta \mathbf{d}$, where $\boldsymbol{\Psi}$ and $\boldsymbol{\Delta}$ are auxiliary operators that contain derivatives of rotation and strain tensors and derivation operators, and can be seen in this latter reference.

Analogously, the external virtual work can be calculated, and it depends on the applied external forces ($\bar{\mathbf{n}}$), moments ($\bar{\mathbf{m}}$) and bi-moment (\bar{B}) (see [7], [8]). An important result, already reported in previous papers ([3], [4], [7], among others) is that the virtual rotations are not directly conjugated with the moments, but, instead, with the so-called pseudo-moments $\bar{\boldsymbol{\mu}} = \boldsymbol{\Gamma}^T \bar{\mathbf{m}}$. The external load can be grouped on the vector $\mathbf{q} = [\bar{\mathbf{n}}, \bar{\boldsymbol{\mu}}, \bar{B}]^T$.

2.3 Constitutive equation

In this work, the model was implemented with the exact (i.e., all strain terms retained) expression for the Saint-Venant's material law. This law is a direct extension of the linear elastic case for the finite deformation case – instead of using the infinitesimal strain tensor, derived for the linear theory, the Green-Lagrange strain tensor \mathbf{E} is used to compute the second Piola-Kirshoff tensor \mathbf{S} . However, for the internal virtual work, the back-rotated first Piola-Kirshoff tensor \mathbf{P}^r is used. Performing the needed conversions, after some algebra the column-vectors of \mathbf{P}^r may be written as follows (see [11])

$$\begin{aligned}\boldsymbol{\tau}_\alpha^r &= \lambda(\mathbf{I}:\mathbf{E})\mathbf{e}_\alpha^r + \mu\mathbf{c}_\alpha + \mu(\mathbf{c}_\alpha \cdot \mathbf{e}_3^r)\boldsymbol{\gamma}_3^r + \lambda(\mathbf{I}:\mathbf{E})p\psi_{,\alpha}\mathbf{e}_3^r + \mu p\psi_{,\beta}(\mathbf{c}_\alpha \cdot \mathbf{e}_\beta^r)\mathbf{e}_3^r, \\ \boldsymbol{\tau}_3^r &= \lambda(\mathbf{I}:\mathbf{E})\mathbf{e}_3^r + \mu\mathbf{c}_3 + \lambda(\mathbf{I}:\mathbf{E})\boldsymbol{\gamma}_3^r + \mu(\mathbf{c}_3 \cdot \mathbf{e}_3^r)\boldsymbol{\gamma}_3^r + \mu p\psi_{,\alpha}(\mathbf{c}_3 \cdot \mathbf{e}_\alpha^r)\mathbf{e}_3^r,\end{aligned}\quad (7)$$

where $\mathbf{I}:\mathbf{E} = \text{tr}(\mathbf{E})$, \mathbf{c}_i represent the column-vectors of the right Cauchy-Green tensor \mathbf{C} , which contains a wide array of products of the elements of $\boldsymbol{\varepsilon}^r$ (see [11] for their analytic expressions) and (λ, μ) are the Lamé constants for the pair $\{\mathbf{S}, \mathbf{E}\}$. Due to the kinematical assumptions, Poisson's effects must be ignored. Therefore, the expressions $\mu = G$ and $\lambda + 2\mu \simeq E$ are used to derive the Lamé's constants from the Young's and shear moduli.

The matrix of elastic tangent moduli \mathbf{D} can also be obtained for this elastic constitutive equation. A detailed description of its components can be found in [11]. It is also important to mention that both $\boldsymbol{\tau}_i^r$ and \mathbf{D} are written in their exact forms, with no simplifications. Strain coupling involving higher-order strain terms can be seen when the exact forms are used (some authors refer to some of those terms as "Wagner terms"). In the context of thin-walled open section members, it is especially important to highlight the coupling between torsional and warping strains (κ_3^r , p and p') with axial and bending strains (η_3^r and κ_α^r).

2.4 Warping function

Many rod models employ the Saint-Venant warping function as the shape function. For linear elastic, or incomplete (simplified) neo-Hookean constitutive equations, the Saint-Venant's torsion inertia (I_t) and Vlasov's warping constant (I_ω) suffice to describe the warping phenomena. However, when the exact expressions of more complex material laws are used, such analytical intermediary results are of little help – numerical integration throughout the cross-section is more practical. Therefore, it is necessary to explicitly evaluate the warping shape function and its derivatives. Due to this, Lago and Campello [11] proposed a shape function that should incorporate both the primary (along the walls' lengths) and secondary (along the walls' thicknesses) warping contributions. For each wall, the function was

$$\psi(x_1, x_2) = \omega(s) + \psi_R(\bar{x}_n, \bar{y}_n), \quad (8)$$

where $\omega(s)$ is the wall's Vlasov's sectorial area (wherein s is the coordinate along the walls' lengths) and ψ_R is the Saint-Venant's torsion warping function for thin rectangular sections (see [11], which uses a polynomial approximation from [14]), relative to the wall's local coordinate system (\bar{x}_n, \bar{y}_n) , defined as in Fig. 1b. For rectangular, I and cruciform cross-sections, eq. (8) recovers very satisfactorily the Saint-Venant's warping function for such thin-walled open sections. However, for the general (mono-symmetric and non-symmetric) case, this does not hold, and the torsional stiffness is greatly overestimated since secondary warping is not correctly addressed. This has not been detected by the authors in [11]. To fix this, we propose here a simple alternative expression that yields a more suitable function, for any thin-walled open section, composed of thin rectangular walls. Accordingly, for each wall n , the warping function is given by

$$\psi(x_1, x_2) = \psi_L(x_1, x_2) + \psi_R(\bar{x}_n, \bar{y}_n), \quad (9)$$

where $\psi_L(x_1, x_2)$ is a linear contribution in (x_1, x_2) , given by

$$\psi_L(x_1, x_2) = -(s_2 - O_n^{x_2})(x_1 - O_n^{x_1}) + (s_1 - O_n^{x_1})(x_2 - O_n^{x_2}) + c_n, \quad (10)$$

where (s_1, s_2) are the coordinates of the section's shear centre and $(O_n^{x_1}, O_n^{x_2})$ the coordinates of the wall's local origin. It is important to highlight that the shear centre is defined by imposing the orthogonality conditions, as presented in [5], [8]. It follows that the warping function is written w.r.t the shear centre. The independent term c_n must only be adjusted so that continuity of the warping function is guaranteed on every wall's intersection. The linear function ψ_L can be interpreted as a result of the axis shift from the wall's local system (where the local Saint-Venant's warping function ψ_R is conceived) to the section's shear centre, rendering the consistent Saint-Venant's warping function for thin-walled open sections. We refer to equations 3.20 and 3.21 from [10] for more details on such axis shift. One interesting observation is that eq. (10) embeds Vlasov's sectorial area, as the value of ψ_L calculated along the wall's midline is precisely that given by $\omega(s)$. Therefore, the only difference between eqs. (8) and (9) are additional terms in (x_1, x_2) in the latter, which represent a linear contribution to the secondary warping. Note that the linear variation of the displacements along the thickness is a common assumption for shell models, and has even been used in other similar rod models (see Gonçalves [15], where only linear terms are present in the warping function). This suggests that ψ_L might be even more important than ψ_R for obtaining the correct behaviour. To illustrate the differences between the functions generated by eqs. (8) and (9), an example of

a channel section is presented in Fig. 2. At first glance, the functions seem very similar. A careful inspection, however, reveals pronounced discrepancies in the secondary warping at the flanges, which greatly affect the Saint-Venant's torsional inertia (I_t) – although not the warping inertia (I_ω). In fact, were eq. (8) to be used for simulations of this section, torsion rotations would be underestimated two hundredfold. The constants are calculated using the standard definitions $I_t = \int_A (x_1^2 + x_2^2 + x_1\psi_{,2} - x_2\psi_{,1})dA$ and $I_\omega = \int_A \psi^2 dA$.

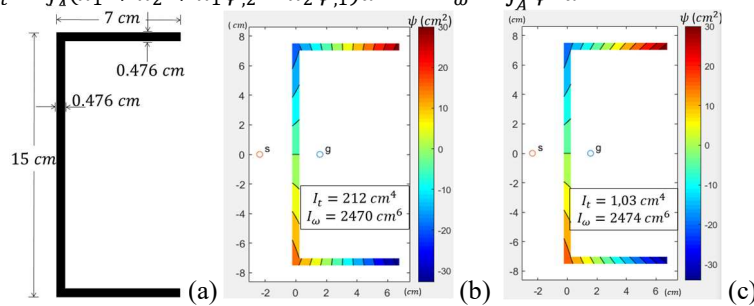


Figure 2. (a) Channel section definition. Warping function with (b) eq. (8) and (c) eq. (9).

3 Numerical Examples

In this section we provide illustrative examples to show the current model's applicability on simple general situations. We consider elastic rods with $E = 200GPa$ and $G = 80GPa$ (except on the C-section of example 3.1, where $E = 210GPa$ was used to be consistent with [16]). The results are compared with reference solutions using kinematically exact rod models with simplified (Vlasov's) warping function and linear elastic material, either from the literature or implemented in PEFSYS (see [8], [10] for details), and also with Ansys's shell models for large deformations and linear elasticity. For examples with pre-critical loading, Vlasov's analytical solutions [2] are also reported for comparison. In order to transpose bifurcation points in post-critical analyses, a load perturbation of 1% of the main load was applied. In all cases, the rods were discretized in 10 linear (i.e., 2-node) elements (the only exception, again, is the C-section from example 3.1, with 30 elements), and the cross-sectional walls in 10×30 integration cells.

3.1 Bending and torsion of beams in small to moderate (pre-critical) loading

This example deals with an I-section, simply supported (torsion rotation restricted at the edges), transversely loaded beam and a channel-section cantilever with a transverse load at the tip (see Fig. 3a). In the first case, the beam axis is placed at the web's mid-height, and in the second case at the intersection of the web and top flange. For the I-beam, a distributed torsion load exists, whereas for the channel cantilever the transverse load is applied outside the shear centre, such as torsion is also expected to occur.

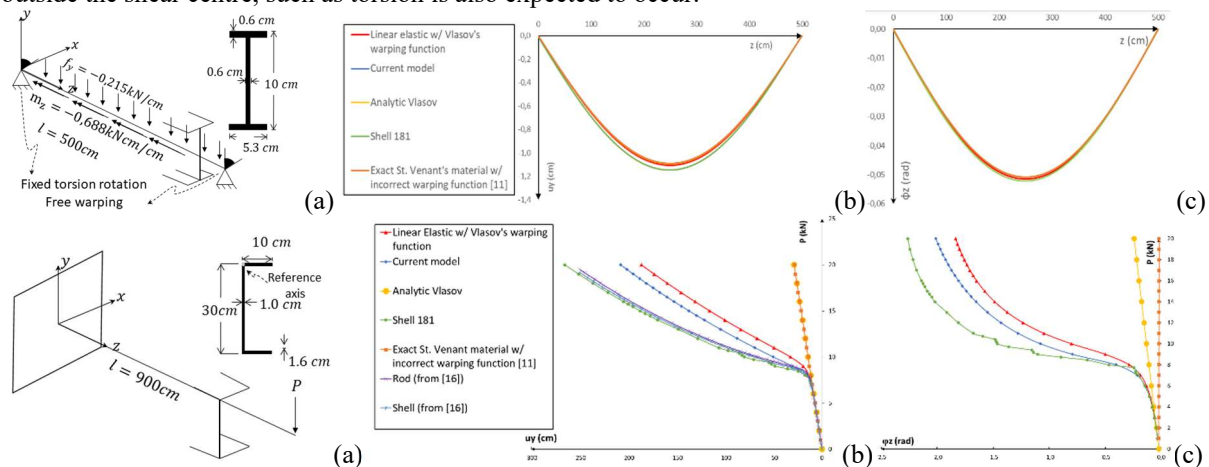


Figure 3. (a) Problem description – example 3.1, (b) vertical displacements (mid-height) and (c) torsion rotation

As it can be seen in Figs. 3b and 3c, results for the I-beam are almost coincident to Vlasov’s analytical solution and to ANSYS’s shell solution. It must be highlighted, though, that this is a bi-symmetric section under small strains and displacements. For the cantilever, in turn, since the section is mono-symmetric and the load eccentric, with the displacements markedly larger, both geometrical and material nonlinearities turn relevant. Up to $P \approx 8$ kN, u_y and θ_z are almost coincident for nearly all models, including the analytical Vlasov’s solution. The exception is [11], which is very stiff for θ_z , as a consequence of the incorrect warping function (there barely is torsion rotation, as anticipated at the end of the previous section). After this load level, there is a change in the load-carrying mechanism and the deformation is intensified (yet, we remark that this is not a case of buckling). Results from [11] do not capture this change. The linear elastic rod model from Campello [10], in turn, proved stiffer than that from Gruttmann et al. [16], despite their kinematical formulation being rather equivalent, suggesting modelling differences on the cross-sectional geometric characterization. This was unexpected and needs to be further investigated. The present model, in turn, with the corrected warping function and higher order strain terms from the exact Saint Venant’s constitutive equation, allowed better results when compared to both [10] and [11], being closer (though not yet similar) to those from shell models.

3.2 Buckling and post-critical analysis of an I-section column and beam

This example deals with the buckling of a (i) compression-loaded and (ii) transversely-loaded I-column and beam, respectively (see Fig. 4a), both with the same cross-section of the example 3.1. As it can be seen in Figs. 4b and 4c, the current model is able to correctly identify the critical load. Comparing with the results from [11], it is evident that the herein proposed warping function provides results that virtually coincide with those from [11] for bi-symmetric I-sections. For the compression case, all models presented nearly the same displacements on the post-critical regime. For the transverse load case, in turn, in the developed large-displacements regime, the influence of high-order strain coupling (notably between torsional and bending strains) in the present model is identified, making the results differ from those of the linear elastic rod and shell models.

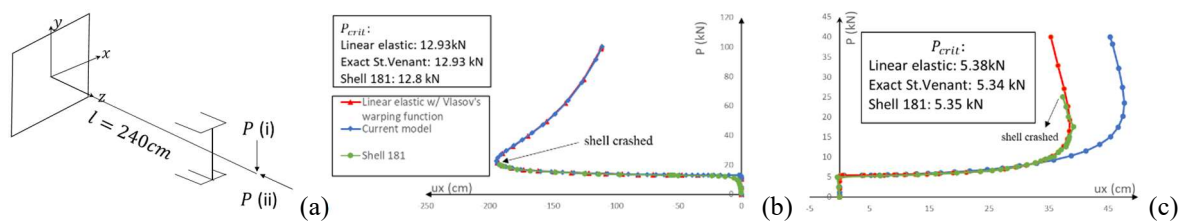


Figure 4. Problem description for example 3.2, lateral displacements for the (a) column and (b) beam

3.3 Torsional buckling of cruciform and T-section columns

This example is the torsional buckling of compressed short columns, with cruciform and T-shaped cross-sections as shown in Fig. 5a. As it can be seen in Figs. 5b and 5c, the rod model with linear elastic material was unable to identify the torsion buckling, whereas the present one with consistent warping function and exact Saint-Venant’s material (with full strain coupling) correctly identified the critical load. It must be said, however, that compared to the shell model, the post-critical torsional response herein obtained is significantly different. One possible explanation is that the shell model is able to capture in-plane cross-sectional deformations (volumetric and distortional changes), which may be relevant in the post-critical regime – especially for such short columns. This issue remains to be further investigated.

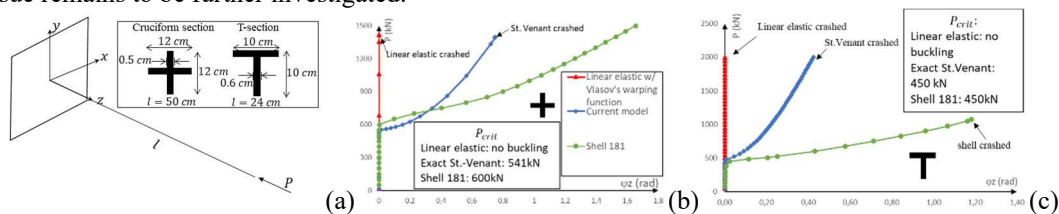


Figure 5. (a) Problem description for example 3.3. Torsion rotation for (a) cruciform section and (b) T-section.

4 Conclusions

The development of a 7-DOF, kinematically exact rod model with secondary-warping and “exact” Saint-Venant’s constitutive equation was achieved. The model was validated in pre-critical loading situations and buckling load determination, as well as in the post-critical regime – including some cases that were not correctly described by simpler rod models. The warping function from [11] was corrected by incorporation of a missing (linear through-the-thickness) term. Plus, the coupling effects between torsion strains and other degrees of freedom proved crucial at the constitutive equation for proper torsional buckling representation. As a next step in this work, besides investigating the small discrepancies observed in example 3.1, an improved constitutive model, with Simo-Ciarlet’s material law, is under development, which shall be more suited to the fully finite-strain situations such as (but not only) more developed post-critical configurations.

Acknowledgements. This work was supported by FAPESP (São Paulo Research Foundation) and CNPq (Conselho Nacional de Desenvolvimento Científico e Tecnológico), under the grants #2021/02042-9 and #307368/2018-1, respectively. The opinions, hypotheses, conclusions and recommendations expressed herein are the sole responsibility of the authors and do not necessarily reflect FAPESP’s and CNPq’s visions.

Authorship statement. The authors hereby confirm that they are the sole liable persons responsible for the authorship of this work, and that all material that has been herein included as part of the present paper is either the property (and authorship) of the authors, or has the permission of the owners to be included here.

References

- [1] S. P. Timoshenko and J. M. Gere, *Theory of Elastic Stability*, 2nd edition. Stanford University: McGRAW-HILL BOOK COMPANY, 1985.
- [2] V. Z. Vlasov, *Thin-walled Elastic Beams*, 2nd ed. Jerusalem: Israel Program for Scientific Translation, 1961.
- [3] J. C. Simo, ‘A finite strain beam formulation. The three-dimensional dynamic problem. Part I’, *Computer Methods in Applied Mechanics and Engineering*, vol. 49, no. 1, pp. 55–70, May 1985, doi: 10.1016/0045-7825(85)90050-7.
- [4] J. C. Simo and L. Vu-Quoc, ‘A three-dimensional finite-strain rod model. part II: Computational aspects’, *Computer Methods in Applied Mechanics and Engineering*, vol. 58, no. 1, pp. 79–116, Oct. 1986, doi: 10.1016/0045-7825(86)90079-4.
- [5] J. C. Simo and L. Vu-Quoc, ‘A Geometrically-exact rod model incorporating shear and torsion-warping deformation’, *International Journal of Solids and Structures*, vol. 27, no. 3, pp. 371–393, 1991, doi: 10.1016/0020-7683(91)90089-X.
- [6] M. A. Crisfield, ‘A consistent co-rotational formulation for non-linear, three-dimensional, beam-elements’, *Computer Methods in Applied Mechanics and Engineering*, vol. 81, no. 2, pp. 131–150, Aug. 1990, doi: 10.1016/0045-7825(90)90106-V.
- [7] P. M. Pimenta and T. Yojo, ‘Geometrically Exact Analysis of Spatial Frames’, *Applied Mechanics Reviews*, vol. 46, no. 11S, pp. S118–S128, Nov. 1993, doi: 10.1115/1.3122626.
- [8] P. M. Pimenta and E. M. B. Campello, ‘Geometrically nonlinear analysis of thin-walled space frames’, *Proceedings of the II ECCM (European Conference on Computational Mechanics)*, 2001, p. 20.
- [9] E. R. Dasambiagio, P. M. Pimenta, and E. M. B. Campello, ‘A finite strain rod model that incorporates general cross section deformation and its implementation by the Finite Element Method’, p. 24, 2009.
- [10] E. M. B. Campello, ‘Análise não-linear de perfis metálicos conformados a frio’, *São Paulo*, p. 106, 2000.
- [11] E. M. B. Campello and L. B. Lago, ‘Effect of higher order constitutive terms on the elastic buckling of thin-walled rods’, *Thin-Walled Structures*, vol. 77, pp. 8–16, Apr. 2014, doi: 10.1016/j.tws.2013.11.001.
- [12] P. M. Pimenta and E. M. B. Campello, ‘A fully nonlinear multi-parameter rod model incorporating general cross-sectional in-plane changes and out-of-plane warping’, *Latin American Journal of Solids and Structures*, p. 22, 2003.
- [13] V. Le Corvec, ‘Nonlinear 3d frame element with multi-axial coupling under consideration of local effects’, Dissertation, University of California, Berkeley, 2012.
- [14] H. F. Silva, ‘Formulação do problema da torção uniforme em barras de seção transversal maciça.’, Mestrado em Engenharia de Estruturas, Universidade de São Paulo, São Paulo, 2005. doi: 10.11606/D.3.2005.tde-20022006-150915.
- [15] R. Gonçalves, ‘An assessment of the lateral-torsional buckling and post-buckling behaviour of steel I-section beams using a geometrically exact beam finite element’, *Thin-Walled Structures*, vol. 143, p. 106222, Oct. 2019, doi: 10.1016/j.tws.2019.106222.
- [16] F. Gruttmann, R. Sauer, and W. Wagner, ‘Theory and numerics of three-dimensional beams with elastoplastic material behaviour’, p. 33.